Hydrothermal fluid evolution in the "Botro ai Marmi" quartz-monzonitic intrusion (Campiglia Marittima, Tuscany, Italy). Evidence from a fluid inclusion investigation

PAOLO FULIGNATI

Dipartimento di Scienze della Terra, Università di Pisa - 56126 Pisa, Italy

E-mail: paolo.fulignati@unipi.it

[*Received 25 July 2017; Accepted 15 February 2018; Associate Editor: Katharina Pfaff*]

Abstract:

The quartz-monzonitic intrusion of "Botro ai Marmi" (Tuscany, Italy) can be considered to be a typical example of an intrusion-centered magmatic hydrothermal system. The evolution of hydrothermal fluids in the "Botro ai Marmi" intrusion was investigated using fluid inclusion analyses to provide suitable physico-chemical constraints on the fluids involved in the late- to postmagmatic hydrothermal activity that affected the intrusion, providing inferences on their origin and variations of temperature and pressure with time.

This work demonstrates that the earliest fluids circulating in the "Botro ai Marmi" intrusion were high-temperature brines exsolved directly from the crystallizing magma. This fluid circulated in the intrusion under lithostatic conditions (P > 90 MPa, T > 540°C). A second evolutionary stage of the magmatic hydrothermal system is marked by the transition from lithostatic (>90 MPa) to

DOI: 10.1180/mgm.2018.116.

hydrostatic dominated conditions (50 to 10 MPa). In this stage the fluids are also interpreted to be mainly orthomagmatic in origin but unmixed in a high-salinity brine and in a low-salinity vapor aqueous phase, at a temperature ranging from about 500°C to 300°C. These fluids were responsible for the potassic alteration facies. At a later stage of hydrothermal evolution, abundant meteoric dominated fluids entered the system and are associated with propylitic alteration. This event marks the transition from a magmatic-hydrothermal system to a typical hydrothermal ("geothermal") system, which can be assumed to be similar to some extent to the nearby active high-enthalpy geothermal system of Larderello. Low-temperature and low-salinity meteoric water-dominated fluids characterize the latest stage of the "Botro ai Marmi" hydrothermal system.

Keywords: Campiglia Marittima, fluid inclusions, hydrothermal fluids, magmatic hydrothermal systems.

Introduction

The Campiglia Marittima area (Southern Tuscany, Italy) has been extensively exploited from the Etruscan period until the 1980's for its abundant Cu-Pb-Zn-Fe-(Ag,Sn) sulfide/oxide skarn mineralization. These are clearly linked to the magmatic hydrothermal systems generated by the emplacement of relatively shallow intrusions and dykes during the Pliocene (Tanelli, *et al.*, 1993 and references therein; Peccerillo and Donati, 2003; Vezzoni *et al.*, 2016). The quartz-monzonitic intrusion (Barberi *et al*, 1967; Poli *et al.*, 1989) of "Botro ai Marmi" (radiometric age of 5.7 Ma, Borsi *et al.*, 1967) is one of the most important magmatic bodies cropping out in the area and can be considered a typical example of an intrusion-centered magmatic hydrothermal system. The development of magmatic hydrothermal systems, associated with intrusive bodies belonging to the Tuscan Magmatic Province, is a quite common feature that has been reported by several authors for other areas of southern Tuscany (Ruggieri and Lattanzi, 1992; Maineri, 1996; Dini *et al.*, 2008; Rossetti and Tecce 2008; Bakker and Schilli, 2016). The emplacement of the "Botro ai Marmi"

intrusion within the Upper Triassic to Lower Liassic carbonates of the Tuscan Nappe prompted the development of a thermometamorphic and metasomatic aureole characterized by the formation of marbles and systems of skarn (Barberi *et al.*, 1967, Leoni and Tamponi, 1991) in which Cu ± Sn ± W mineralization occurred (Tanelli *et al.*, 1993).

This work is based on a detailed fluid inclusion study and aims to provide strong physico-chemical constraints on the evolution of the fluids involved in the late- and post-magmatic hydrothermal activity that affected the "Botro ai Marmi" intrusion, providing inferences on their origin and variation of temperature and pressure with time. These results assume particular relevance if the exposed "Botro ai Marmi" magmatic hydrothermal system is considered to some extent as a fossil analogue to the active high-enthalpy Larderello geothermal system, which is located only few kilometers eastward.

Geological framework

The study area is located in the inner zone of the Northern Apennines (Fig. 1), an arc-shaped collisional belt originating from the convergence and subsequent collision (Cretaceous-Early Miocene) between the Adria and the Sardinia-Corsica microplates. This process resulted in stacking of tectonic units from the paleogeographic domains of the Inner Northern Apennines. The resulting thrust-belt complex is made up of the tectonic units, from top to bottom (Carmignani *et al.*, 1994): 1) Ligurian and Subligurian units, which consist of remnants of Jurassic oceanic crust (low-grade metabasic and mafic rocks), its Upper-Jurassic-Lower-Cretaceous pelagic sedimentary cover and overlying Cretaceous-Oligocene arenaceous and calcareous, turbidite involved in multiple thrust sheets; 2) Tuscan units, including sedimentary (Tuscan Nappe, formed by shallow-marine pelagic carbonaceous/carbonaceous siliceous and pelagic terrigenous formations) and metamorphic (Monticiano-Roccastrada Unit, a mainly continental siliciclastic formation) sequences ranging in age from Paleozoic to Early Miocene.

The original Oligocene architecture of the thrust belt was modified by Neogene post-orogenic extensional tectonics (Carmignani *et al.*, 1994; Brogi *et al.*, 2005; Brogi and Liotta, 2008). Since the early Pliocene, high-angle normal and strike-slip faults dissected the extensional detachments forming NNW-SSE trending basins of Pliocene-Quaternary age that were successively filled by marine and continental sediments (Martini and Sagri, 1993). Extensional structures developed contemporaneously with the emplacement of acidic magmatic bodies at shallow crustal levels (Tuscan Magmatic Province; Innocenti *et al.*, 1992; Peccerillo, 2001; Peccerillo and Donati, 2003), with an overall eastward migration, following the extensional deformation (Serri *et al.*, 1993; Jolivet *et al.*, 1998; Rossetti *et al.*, 2000, 2008; Acocella and Rossetti, 2002; Dini *et al.*, 2005). Intrusive rocks crop out mainly in the Tuscan archipelago (Monte Capanne, Porto Azzurro, Montecristo, and Giglio intrusions) and along the coastal area of southern Tuscany (Campiglia and Gavorrano granites, Rocchi *et al.*, 2003), whereas, buried intrusions occur in the subsurface of the Larderello geothermal field. The emplacement of these magmatic bodies produced the superheating of hosting rocks accompanied by intense circulation of hydrothermal fluids within the permeable substratum and is at the origin of the wide pyrite, iron, base metals, mercury, antimony and minor silver-gold ore mineralization and of the active high-enthalpy geothermal systems (Larderello and Mt. Amiata) that characterize southern Tuscany (Marinelli, 1963, 1969; 1983; Tanelli, 1983; Lattanzi, 1999; Bellani *et al.*, 2004).

The Campiglia Ridge, located in the westernmost part of the Colline Metallifere area, is composed of rocks of the Tuscan Nappe sequence and is bordered to the west and east by N-S and NW-SE trending faults (Figs 1, 2), respectively (Rossetti *et al.*, 2000). The quartz-monzonitic intrusion of "Botro ai Marmi" crops out on the western edge of the ridge (Fig. 2) and is associated with the development of a wide thermometamorphic and metasomatic aureola characterized by the occurrence of marble and skarn.

Hydrothermal alteration

The "Botro ai Marmi" intrusion was affected by a widespread hydrothermal alteration, which occurred through three main stages. 1) The earliest alteration was prevalently potassic and is characterized by a pervasively developed mineral assemblage composed of K-feldspar + irregularly shaped crystals of phlogopite (Fig. 3a, Table 1). This initial potassic stage was followed by 2) a propylitic alteration that produced quartz + adularia + chlorite + illite + mixed sulfides veins cross-cutting the intrusive body (Fig. 3b, Table 1), and a pervasive alteration of quartz-monzonite partially overprinting the potassic facies (Figs 3a,c). Galena, pyrite, arsenopyrite, cassiterite, uraninite and bismuthinite are associated with the propylitically altered veins. 3) The latest stage of the hydrothermal alteration is represented by the supergene calcite (Fig. 3d) and iron-oxide-hydroxide-bearing massive deposits ("brucioni") that occur around the upper part of the intrusion outcrop as late alteration and re-mobilization of the primary skarn mineralization, as also reported by Conticini *et al*. (1980) and Tanelli *et al.* (1993).

Fluid inclusion investigation

Analytical methods

A fluid inclusion investigation was carried out on quartz crystals from late magmatic veins in the "Botro ai Marmi" intrusion, and on calcite crystals from the supergenic iron-oxide-hydroxide bearing deposits. The reconnaissance survey of fluid inclusions was undertaken in over 30 samples, to assess the spatial variability of fluid inclusion characteristics, and 5 doubly polished thin sections (100-300 μm thick) were prepared for petrography and microthermometric determinations. Measurements were made using a Linkam THMS 600 heating-freezing stage (Earth Sciences Department, University of Pisa). The accuracy of measurements was ±2°C at 398°C controlled by the melting point of $K_2Cr_2O_7$, ±0.1°C at 0°C and ±0.2°C at -56.6°C controlled by using certified pure water and CO_2-bearing synthetic fluid inclusions (Synthetic Fluid Inclusion Reference Set, Bubbles Inc., USA). The rate of heating and freezing experiments was varied as a function of the

rate of transformations in the inclusions and ranged from 2 to 30°C/min. Salinities of fluid inclusions were calculated from final ice-melting, halite dissolution and clathrate melting temperatures using the equations of Sterner *et al.* (1988) and Bodnar (1993) for the H_2O-NaCl system, and Darling (1991) for the H_2O-CO_2-NaCl system respectively.

Results

Petrography and texture of fluid inclusions

Fluid inclusions hosted within quartz have generally ellipsoidal morphologies and in some cases display negative crystal morphologies, whereas those hosted within calcite are highly irregular in shape. Some inclusions (particularly those hosted within calcite) display variable liquid to vapor ratios suggesting that they were affected by post-entrapment processes (i.e., necking down or stretching); as a consequence, their microthermometric data are meaningless and are not reported. The classification of fluid inclusion types observed in this study is primarily based on phase proportions at room temperature. All descriptions strictly refer to fluid inclusion assemblages (FIAs, Goldstein and Reynolds, 1994), avoiding single isolated fluid inclusions, and the types of fluid inclusions in each FIA were noted. A close examination of the appearance of fluid inclusions at room temperature has allowed the identification of three main types of fluid inclusions: multiphase (liquid + vapor + daughter minerals) inclusions (LVHS), liquid rich at room temperature (hosted within quartz crystals); two-phase (liquid + vapor) inclusions (LV), liquid rich at room temperature (hosted within either quartz and calcite crystals); and two-phase (vapor + liquid) inclusions (VL), vapor rich at room temperature (hosted within quartz crystals).

LVHS inclusions are 20-70 μm in size and consist of liquid + vapor + halite + sylvite + other solids (Fe-Cu-Sn-Zn-As sulfides, scheelite, fluorite, barite, carbonates, as reported in Caiozzi *et al.* 1998 on the basis of SEM-EDS analysis on opened LVHS inclusions hosted within the same samples considered for the present study). Based on the number and type of the solids and the distribution of

fluid inclusions types in the quartz crystals, we have further classified LVHS fluid inclusions into two subtypes. Subtype $LVHS_1$ inclusions are randomly distributed inside the quartz crystals and often form isolated clusters (Fig. 4a), and hence bear an unambiguous primary origin (Goldstein, 2003). $LVHS_1$ inclusions are characterized by the presence of halite + sylvite + several other solids (Figs 4b,c). Some of them have tabular and elongated habits and show birefringence. Opaque minerals are also present. Vapor bubbles occupy <30% of the inclusions by volume, whereas the solid phases occupy about 60-70%. Subtype $LVHS_2$ inclusions are generally distributed along healed fractures in quartz suggesting a secondary origin (Goldstein, 2003) and are often spatially associated with vapor-rich inclusions (Figs 4d, e). They contain halite + sylvite ± one or two solids; opaque minerals are very rare. The bubble takes up ~20% of the inclusion volume, whereas the solids are ~50%.

LV inclusions consist of liquid + vapor with the liquid phase volumetrically dominant. These fluid inclusions are generally between 10 and 30 μm in size and were commonly observed in quartz crystals always forming secondary trails. We have further classified LV fluid inclusions hosted in quartz into two subtypes on the basis of the degree of fill. In LV_1 inclusions the vapor bubbles are variable in size from 30% to 40% of inclusion volumes (Fig. 4f), whereas in LV_2 inclusions the vapor bubbles occupy about 10% (Fig. 4g). LV_1 and LV_2 inclusions show a distinct homogenization temperature. Textural relationships suggest that LV_2 inclusions postdate the LV_1 population. LV inclusions in supergene calcite (LV_3) are rare and have an irregular shape, and the bubbles fill about 30% of the inclusion (Fig. 4h).

VL inclusions contain vapor + liquid ± CO_2 (gas). Vapor bubble consists of >90% of the inclusion volume. They are generally between 10 and 30 μm in size and mostly occur spatially associated with $LVHS_2$ inclusions (Figs 4d,e). Because of the small amount of liquid phase, we were able to study only few inclusions of this type. No daughter crystals or liquid CO_2 were observed.

Microthermometric measurements

The results of the microthermometric investigation are reported in Figs 5a,b and 6a,b and in Table 2. Freezing runs were performed on both liquid-rich and vapor-rich inclusions. Fluid inclusions freeze to ice upon cooling below -30/-40°C, as clearly observed by the sudden shrinkage of the vapor bubble. During warming, the temperature of initial melting of ice (eutectic temperature, T_e) was measured for all three types of inclusions (LVHS, LV and VL). The T_e in VL inclusions was difficult to determine because of their low degree of filling. In VL inclusions, clathrate formation was often observed during freezing runs. Clathrates melt between 2°C and 10°C. The T_e in LVHS, LV_1 and LV_3 inclusions is between –35°C and -40°C, suggesting high concentrations of divalent cations (i.e., Ca, Mg and Fe) in addition to Na and K (Crawford, 1981). LV_2 inclusions show a T_e of about -21/-23°C, suggesting that NaCl ± KCl are the principal salts in solution.

Upon heating, $LVHS_1$ inclusions homogenize mainly by halite dissolution. The vapor bubble homogenizes (T_h) between 245°C and 522°C, and the dissolution of halite (T_s) occurs between 300°C and 575°C corresponding to salinities of 38-70 wt% $NaCl_{equiv.}$. The dissolution temperature of sylvite ($T_{s\text{-}KCl}$) ranges from 100°C to 455°C. The composition of $LVHS_1$ fluid inclusions as deduced from halite and sylvite dissolution temperatures, when modeled in the system NaCl-KCl-H_2O (Fig. 7), appear to define a linear trend similar in many respects to the "halite trend" of Cloke and Kesler (1979). The slope corresponds to an average K/Na atomic ratio of approximately 0.72. However, it must be taken into account that this provides a very rough estimate of the composition of the fluid, as it ignores the possible effect of other ions on the solubility of halite and sylvite (Roedder, 1984; Stefanini and Williams-Jones, 1996; Hezarkhani and Williams-Jones, 1998).

In $LVHS_2$ inclusions, halite dissolves in the range 240-470°C, corresponding to salinities between 34 and 56 wt% $NaCl_{equiv.}$, whereas the final homogenization occurs by bubble disappearance at T_h ranging between 280°C and 510°C. Very few data on dissolution temperature of sylvite have been obtained, showing a range between 140°C and 250°C.

The temperature of final melting of ice (T_{fmi}) in LV_1 inclusions ranges from –1.3°C to –12.2°C, corresponding to salinities of 2.2 and 16.1 wt% $NaCl_{equiv.}$ with a mode around 5 wt% $NaCl_{equiv.}$. The T_h is between 250°C and 400°C with the mode at about 300°C.

In LV_2 inclusions, the T_{fmi} value varies from -0.1°C to –1.5°C equating to salinities between 0.2 and 2.5 wt% $NaCl_{equiv.}$ with the mode at 0.5 wt% $NaCl_{equiv.}$. The vapor bubbles homogenize to liquid between 195°C and 265°C with the mode at about 240°C.

LV_3 fluid inclusions investigated in supergene calcite samples have T_h between 100°C and 165°C with a mode at about 130°C. Unfortunately, few freezing experiments have been done on these latter inclusions because of the problem of stretching and subsequent decrepitation of inclusions. However, the few obtained data indicate low salinity (around 0.1/0.2 wt% $NaCl_{equiv.}$) of the trapped fluid.

VL fluid inclusions exhibit T_h in the range 328-488°C. These inclusions often display clathrate formation during freezing runs. Clathrate melting occurs between +2°C and +10°C, corresponding to salinities in the range 2 to 17 wt% $NaCl_{equiv.}$.

Discussion

The petrographic and microthermometric data obtained from the analysis of the different types of fluid inclusions (LVHS, LV and VL) provide a basis for a compositional and thermobarometric characterization of the fluids that circulated in the "Botro ai Marmi" intrusion, from the early to the latest stage of hydrothermal evolution. Several populations of fluid inclusions have been identified in the "Botro ai Marmi" intrusion, providing evidence for several events of fluid entrapment during the late stages of granite crystallization and during its hydrothermal history.

We propose that both fluids represented by $LVHS_1$ and $LVHS_2$ + VL inclusions were mainly orthomagmatic. $LVHS_1$ primary inclusions can be considered as high-salinity fluids generated directly by separation of brine (in this work the term "brine" is referred to aqueous fluids having a salinity in excess of 30 wt% $NaCl_{equiv.}$) from a silicate melt, and textural evidence suggests that the

high-salinity brine trapped in these inclusions was the earliest to circulate in the hydrothermal system. It is unlikely that these saline fluids were generated through formation of immiscible aqueous vapor and brine, because of the lack of a coexisting population of vapor-rich inclusions. The homogenization of $LVHS_1$ fluid inclusions by halite dissolution furthermore constrains the inclusion fluid to have been trapped in the liquid-stable, vapor-absent field (Cline and Bodnar, 1994). This indicates that these dense brines, at the time of trapping, did not coexist at equilibrium with a low-density (vapor) fluid phase. The conclusion that $LVHS_1$ fluid inclusions represent a brine directly exsolved from magma is also based on the fact that their compositions delineate a so-called halite trend on a NaCl-KCl-H_2O diagram (Fig. 7), similar to those reported for other magmatic-hydrothermal systems (Eastoe, 1978; Ahmad and Rose, 1980; Wilson *et al.*, 1980; Quan *et al.*, 1987; Stefanini and Williams-Jones, 1996; Hezarkhani and Williams-Jones, 1998). These trends have been interpreted by Cloke and Kesler (1979) as being due to early saturation of the fluid with halite and subsequent trapping of the fluid over an interval of cooling.

To interpret trapping conditions for these inclusions, a dense cluster of data points, representing high-salinity and high-temperature fluids (average T_h = 480°C and T_s = 540°C equating to salinity of 65 wt% $NaCl_{equiv.}$), has been selected for a detailed analysis (Fig. 8). If these inclusions are modeled by the system NaCl-H_2O, the halite dissolution temperatures can be used to estimate minimum temperature and pressure of entrapment. The slopes of halite liquidus and the iso-Th line were determined by extrapolating the data of Bodnar (1994). The iso-Th line intersects the liquidus [L(65)+H] at a temperature of 540°C and a pressure of about 90 MPa (Fig. 9). The same pressure (around 90 MPa) has been also calculated using the Microsoft Excel spreadsheet HOKIEFLINCS-H2O-NACL (Steele-MacInnis *et al.*, 2012), which incorporates the new data of Becker *et al.* (2008) and the equations of Lecumberri-Sanchez *et al.* (2012). This value of pressure corresponds to a depth of about 3 km, assuming that the pressure is lithostatic (see below). These data are in good agreement with the temperature and pressure estimation reported by Barberi *et al.* (1967) and Rocchi *et al.* (2003). We assume that the high-salinity and high-temperature magmatic fluid,

trapped in $LVHS_1$ fluid inclusions, circulated in the "Botro ai Marmi" hydrothermal system under lithostatic pressure conditions because, as indicated by Fournier (1991, 1999), intrusions of magmatic bodies at relatively shallow depth (2 to 6 km) commonly result in a large volume of rocks attaining temperatures sufficiently hot (>400°C) to behave in a plastic manner. At these conditions, the least principal stress is the lithostatic load and the fluids exsolved from crystallizing magma typically accumulate at lithostatic pressure, and are not directly connected with the, eventually present, overlying meteoric-dominated fluid reservoirs. Similar characteristics are also found in other intrusive complexes of southern Tuscany such as Larderello and Elba island (Cathelineau *et al*., 1994; Rossetti and Tecce, 2008; Dini *et al.,* 2008; Fulignati, 2017).

$LVHS_2$ and VL inclusions are commonly associated spatially and can be interpreted as resulting from the formation of immiscible low-density aqueous vapor and high-density brine following an unmixing process (a sort of "boiling"). These inclusions postdate $LVHS_1$ population. As these fluid inclusions are representative of an unmixed fluid, the T_h of the inclusions corresponds to the real fluid-trapping temperature, which ranges from about 500°C to 300°C. These temperature conditions are near the ductile to brittle transition of quartz–feldspar-rich rocks, where magmatic fluids are most likely to change from lithostatic to hydrostatic pressure (Fournier, 1999; Landtwing *et al.*, 2005). Based on data of Chou (1987) for the $NaCl\text{-}H_2O$ system, we can estimate the pressure of entrapment (Fig. 10), which varies between 50 and 10 MPa. We conclude that $LVHS_2$ and VL fluid inclusions record a later stage in the evolution of the "Botro ai Marmi" magmatic-hydrothermal system than that of $LVHS_1$ fluid inclusions. In this stage, the conditions were closer to hydrostatic; orthomagmatic fluid was released into new fractures and therefore expanded to lower pressure so that phase separation occurred. This stage probably marks also the initial inflow of external (meteoric) fluids in the system with subsequent mixing with orthomagmatic fluids. These features are compatible with the evolving fluid regime (from dominantly lithostatic to hydrostatic pressure conditions) and rheological environment (from ductile to brittle) expected in cooling magmatic–

hydrothermal systems (Fournier, 1999). We assume LVHS inclusions as representative of the fluids involved in the genesis of potassic alteration.

Secondary LV_1 and LV_2 fluid inclusions record a mainly meteoric water-dominated hydrothermal system stage at 240°C-310°C and are responsible of the propylitic alteration that characterizes the veins cross-cutting the intrusion. The general decrease in salinity from 16 down to <1 wt% $NaCl_{equiv.}$ in LV_1 and LV_2 fluid inclusions and the corresponding decrease in homogenization temperature (Fig. 11) suggest that meteoric water may have undergone mixing with late magmatic fluids to variable degrees. This meteoric water-dominated stage can be assimilated with the development of a typical paleo-geothermal system in the area, which can be assumed to be similar to some extent to the active high-enthalpy geothermal system of Larderello, extensively exploited for power production, located only a few km east of the "Botro ai Marmi" intrusion. Several works in fact revealed a complex evolution of the fluids that circulated in the subsoil of the Larderello geothermal system, from an early stage, dominated by magmatic and thermometamorphic fluids, associated with the emplacement of granitic intrusions, to the present-day fluids prevalently of meteoric origin (Valori *et al.*, 1992; Cathelineau *et al*., 1994; Ruggieri *et al.*, 1999; Ruggieri and Gianelli, 1999; Boyce *et al.*, 2003; Fulignati, 2017), which is very similar to what we observed in this study on hydrothermal fluid circulation associated with the "Botro ai Marmi" intrusion. In this view, the fossil hydrothermal system of "Botro ai Marmi" may be therefore envisaged as an exposed proxy of the active Larderello geothermal system.

LV_3 inclusions in supergene calcite record the latest and relatively low-temperature stage (100-160°C) of the hydrothermal system linked to the "Botro ai Marmi" intrusion.

Concluding remarks

Fluid inclusion investigation in the "Botro ai Marmi" intrusion allowed tracing of the history of the evolution of the hydrothermal fluids that circulated in the quartz-monzonitic body and its surroundings.

1) The earliest high-salinity and high-temperature fluids to circulate in the "Botro ai Marmi" intrusion are interpreted to have been derived by direct exsolution of a high-density phase (brine) from the crystallizing magma ($LVHS_1$ inclusions). This fluid circulated in the intrusion under lithostatic conditions.

2) The occurrence of $LVHS_2$ and VL fluid inclusion populations marks the transition to an intermediate evolutionary stage of the magmatic-hydrothermal system, in which we have the development of a system with progressively more open fractures and the transition from lithostatic- (>90 MPa) to hydrostatic-dominated conditions (50 to 10 MPa). These fluid inclusions are also interpreted to represent an orthomagmatic fluid that unmixed in a high-salinity brine and in a low-salinity vapor aqueous phase. However, part of these fluids, which circulated at a lower temperature than that represented by $LVHS_1$ inclusions, may have begun to mix and dilute with meteorically derived external fluids. The fluids represented by $LVHS_1$ and $LVHS_2$ inclusions were responsible for the potassic alteration facies.

3) At a later stage of the hydrothermal evolution, abundant meteoric-dominated external fluids entered the system along a network of fractures. These fluids are recorded by two-phase low-salinity LV_1 and LV_2 fluid inclusions that are associated with the development of propylitic alteration. This event marks the transition from a magmatic-hydrothermal system to a typical hydrothermal (“geothermal”) system, probably similar to the nearby active high-enthalpy geothermal system of Larderello.

4) As testified by LV_3 fluid inclusions, the latest stage of the "Botro ai Marmi" hydrothermal system is represented by the circulation of low-temperature and low-salinity meteoric water-dominated fluids, which are the likely mineralizing agents that produced the iron-oxide-hydroxide bearing deposits.

Acknowledgements

Prof Richard Henley is sincerely acknowledged for his constructive review of the manuscript. I would like to thank also an anonymous editorial board member of the Journal whose suggestions helped to improve the clarity of the manuscript. This research was supported by a University of Pisa grant PRA 2016 to Chiara Montomoli.

References

Acocella, V. and Rossetti, F. (2002) The role of extensional tectonics at different crustal levels on granite ascent and emplacement: an example from Tuscany (Italy). *Tectonophysics*, **354**, 71-83

Ahmad, S.N. and Rose, A.W. (1980) Fluid inclusions in porphyry and skarn ore at Santa Rita, New Mexico. *Economic Geology*, ***75***, 229-250

Barberi, F., Innocenti, F. and Mazzuoli, R. (1967) Contributo alla conoscenza chimico-petrologica e magmatologica delle rocce intrusive, vulcaniche e filoniane del Campigliese (Toscana). *Memorie della Società Geologica Italiana*, **6**, 643-681

Bakker, R.J. and Schilli, S.E. (2016) Formation conditions of leucogranite dykes and aplite-pegmatite dykes in the eastern Mt. Capanne plutonic complex (Elba, Italy): fluid inclusion studies in quartz, tourmaline, andalusite and plagioclase. *Mineralogy and Petrology*, **110**, 43-63.

Becker, S.P., Fall, A. and Bodnar, R.J. (2008) Synthetic fluid inclusions. XVII PVTX properties of high salinity H_2O-NaCl solutions (>30 wt % NaCl): Application to fluid inclusions that homogenize by halite disappearance from porphyry copper and other hydrothermal ore deposits. *Economic Geology*, **103**, 539-554

Bellani, S., Brogi, A., Lazzarotto, A., Liotta, D. and Ranalli, G. (2004) Heat flow, deep temperatures and extensional structures in the Larderello Geothermal Field (Italy): constraints on geothermal fluid flow. *Journal of Volcanology and Geothermal Research,* **132**, 15-29

Bodnar, R.J. (1993) Revised equation and table for determining the freezing point depression of H_2O-NaCl solutions. *Geochimica et Cosmochimica Acta,* **57**, 683-684

Bodnar, R.J. (1994) Synthetic fluid inclusions: XII. The system H_2O-NaCl. Experimental determination of the halite liquidus and isochores for a 40 wt. % NaCl solution. *Geochimica et Cosmochimica Acta,* **58**, 1053-1063

Borsi, S., Ferrara, G. and Tongiorgi, E. (1967) Determinazione con il metodo del K/Ar delle età delle rocce magmatiche della Toscana. *Bollettino della Società Geologica Italiana,* **86**, 403-410

Boyce, A.J., Fulignati, P. and Sbrana, A. (2003) Deep hydrothermal circulation in the granite intrusion beneath Larderello geothermal area (Italy): constraints from mineralogy, fluid inclusions and stable isotopes. *Journal of Volcanology and Geothermal Research,* **126**, 243-262

Brogi, A., Lazzarotto, A., Liotta, D. and Ranalli, G. CROP18 Working Group (2005) Crustal structures in the geothermal areas of southern Tuscany (Italy): insights from the CROP18 deep seismic reflection lines. *Journal of Volcanology and Geothermal Research,* **148**, 60-80

Brogi, A. and Liotta, D. (2008) Highly extended terrains, lateral segmentation of the substratum, and basin development: the Middle-Late Miocene Radicondoli Basin (inner northern Apennines, Italy). *Tectonics*, **27**, TC 5002, doi: 10.1029/2007TC002188

Caiozzi, F., Fulignati, P., Gioncada, A. and Sbrana, A. (1998) Studio SEM-EDS dei minerali figli nelle inclusioni fluide del granito di Botro ai Marmi (Campiglia Marittima) e possibili implicazioni minerogenetiche. *Atti della Società Toscana di Scienze Naturali,* **105**, 65-73

Carmignani, L., Decandia, F.A., Disperati, L., Fantozzi, P.L., Lazzarotto, A., Liotta, D. and Meccheri, M. (1994) Tertiary extensional tectonics in Tuscany (Northern Apenines, Italy). *Tectonophysics,* **238**, 295-315

Cathelineau, M., Marignac, C., Boiron, M.C., Gianelli, G. and Puxeddu, M. (1994) Evidence for Li-rich brines and early magmatic fluid-rock interaction in the Larderello geothermal system. *Geochimica et Cosmochimica Acta,* **58**, 1083-1099

Chou, I.M. (1987) Phase relations in the system NaCl-KCl-H_2O. III: Solubilities of halite in vapor-saturated liquids above 445°C and redetermination of phase equilibrium properties in the system NaCl-H_2O to 1000°C and 1500 bars. *Geochimica et Cosmochimica Acta,* **51**, 1065-1075

Cline, J.S. and Bodnar, R.J. (1994) Direct evolution of brine from a crystallizing silicic melt at the Questa, New Mexico, molybdenum deposit. *Economic Geology,* **89**, 1780-1802

Cloke, P.L. and Kesler, S.E. (1979) The halite trend in hydrothermal solutions. *Economic Geology,* **74**, 1823-1831

Conticini, F., Menchetti, S., Sabelli, C. and Trosti Ferroni, R. (1980) Minerali di alterazione dei giacimenti a solfuri misti di Campiglia Marittima (Toscana). *Rendiconti della Società Italiana di Mineralogia Petrografia,* **36**, 295-308

Crawford, M.L. (1981) Phase equilibria in aqueous fluid inclusions. In: Hollister, L.S., & Crawford, M.L. (Eds), Short Course in Fluid Inclusions: Application to Petrology. *Mineralogical Association of Canada,* **6**, pp. 75-100

Darling, R.S. (1991) An extended equation to calculate NaCl contents from final clathrate melting temperatures in H_2O-CO_2-NaCl fluid inclusions: Implications for P-T isochore location. *Geochimica et Cosmochimica Acta,* **55**, 3869-3871

Dini, A., Gianelli, G., Puxeddu, M. and Ruggieri, G. (2005) Origin and evolution of Pliocene–Pleistocene granites from the Larderello geothermal field (Tuscan Magmatic Province, Italy). *Lithos,* **81**, 1–31

Dini, A., Mazzarini, F., Musumeci, G. and Rocchi, S. (2008) Multiple hydro-fracturing by boron-rich fluids in the Late Miocene contact aureole of eastern Elba Island (Tuscany, Italy). *Terra Nova*, **20**, 318-326

Eastoe, C.G. (1978) A fluid inclusion study of the Panguna porphyry copper deposit, Bouganville, Papua New Guinea. *Economic Geology*, **73**, 721-748

Fournier, R.O. (1991) The transition from hydrostatic to greater than hydrostatic fluid pressure in presently active continental hydrothermal systems in crystalline rock. *Geophysical Research Letters*, **18**, 955-958

Fournier, R.O. (1999) Hydrothermal process related to movement of fluid from plastic into brittle rock in the magmatic-epithermal environment. *Economic Geology*, **94**, 1193-1211

Fulignati, P. (2017) Fluid inclusion evidence on the direct exsolution of magmatic brines from a granite intrusion beneath the eastern sector of Larderello geothermal field (Italy). *Periodico di Mineralogia*, 86, 201-211

Goldstein, R.H. (2003) Petrographic analysis of fluid inclusions. In: Samson, I., Anderson, A., & Marshall D. (Eds), Fluid inclusions analysis and interpretation. *Mineralogical Association of Canada, Short Course*, **32**, pp. 9-53

Goldstein, R.H. and Reynolds, T.J. (1994) Systematics of fluid inclusionsin diagenetic minerals. *Society for Sedimentary Geology Short Course* 31, pp. 1-199

Hezarkhani, A. and Williams-Jones, A.E. (1998) Controls of alteration and mineralization in the Sungun porphyry copper deposit, Iran: Evidence from fluid inclusions and stable isotopes. *Economic Geology*, **93**, 651-670

Innocenti, F., Serri, G., Ferrara, G., Manetti, P. and Tonarini, S. (1992) Genesis and classification of the rocks of the Tuscan Magmatic Province: thirty years after Marinelli's model. *Acta Vulcanologica*, **2**, 247-265

Jolivet, L., Faccenna, C., Goffè, B., Mattei, M., Brunet, C., Rossetti, F., Cadet, J.P., Funiciello, R., Theye, T., Storti, F. and D'Agostino, N. (1998) Mid-crustal shear zones in postorogenic

extension: example from the Northern Apennines case. *Journal of Geophysical Research*, **103**, 12123-12150

Landtwing, M.R., Pettke, T., Halter, W.E., Heinrich, C.A., Redmond, P.B., Einaudi, M.T. and Kunze, K. (2005) Copper deposition during quartz dissolution by cooling magmatic-hydrothermal fluids: The Bingham porphyry. *Earth and Planetary Science Letters*, **235**, 229-243.

Lattanzi, P. (1999) Epithermal precious metal deposits of Italy - an overview. *Mineralium Deposita*, **34**, 630-638

Lecumberri-Sanchez, P., Steele-MacInnis, M. and Bodnar, R.J. (2012) A numerical model to estimate trapping conditions of fluid inclusions that homogenize by halite disappearance. *Geochimica et Cosmochimica Acta*, **92**, 14-22

Leoni, L. and Tamponi, M. (1991) Thermometamorphism in the Campiglia Marittima aureole (Tuscany, Italy). *Neues Jahrbuch Mineralogie Meinshafte*, **1991(4)**, 145-157

Maineri, C. (1996) Magmatic-hydrothermal system of the Isola del Giglio granitoid intrusion, Southern Tuscany. *Plinius*, **15**, 103-108

Marinelli, G. (1963) L'energie geothermique en Toscane. *Annales de la Société Géologique Belgique*, **85**, 417-438

Marinelli, G. (1969) Some geological data on the geothermal areas of Tuscany. *Bullettin of Volcanology*, **33**, 19-34

Marinelli, G. (1983) Il magmatismo recente in Toscana e le sue implicazioni minerogenetiche. *Memorie della Società Geologica Italiana*, **25**, 111-124

Martini, I.P. and Sagri, M. (1993) Tectonosedimentary characteristics of Late Miocene-Quaternary extensional basins of the Nothern Apennines. *Earth Science Review*, **34**, 197–233

Peccerillo, A. (2001) Geochemistry and petrogenesis of Quaternary magmatism in central-southern Italy. *Geochemistry International*, **39**, 521-535

Peccerillo, A. and Donati, C. (2003) The Tuscan Magmatic Province. *Periodico di Mineralogia,* **72**, 27-39

Poli, G., Manetti, P. and Tommasini, S. (1989) A petrological review on Miocene-Pliocene intrusive rocks from Southern Tuscany and Tyrrhenian Sea (Italy). *Periodico di Mineralogia,* **58**, 109-126

Quan, R.A., Cloke, P.L. and Kesler, S.E. (1987) Chemical analyses of halite trend inclusions from the Granisle porphyry copper deposit, British Columbia. *Economic Geology,* **82**, 1912-1930

Rocchi, S., Dini, A., Mazzarini, F. and Poli, G. (2003) Campiglia Marittima and Gavorrano intrusive magmatism. *Periodico di Mineralogia*, **72**, 127-132.

Roedder, E. (1984) Fluid inclusions. *Reviews in Mineralogy*, **12**, 644 p

Rossetti, F. and Tecce, F. (2008) Composition and evolution of fluids during skarn development in the Monte Capanne thermal aureole, Elba Island, central Italy. *Geofluids,* **8**, 167-180.

Rossetti, F., Faccenna, C., Acocella, V., Funiciello, R., Jolivet, L. and Salvini, F. (2000) Pluton emplacement in the northern Tyrrhenian Sea area (Italy). *Journal of the Geological Society of London Special Publication,* **174**, 55–77

Rossetti, F., Balsamo, F., Villa, I.M., Bouybaouenne, M., Faccenna, C. and Funiciello, R. (2008) Pliocene-Pleistocene HT-LP metamorphism during multiple granitic intrusions in the southern branch of the Larderello geothermal field (southern Tuscany, Italy). *Journal of the Geological Society of London,* **165**, 247-262

Ruggieri, G. and Lattanzi, P. (1992) Fluid inclusion studies on Mt. Capanne pegmatites, Isola d'Elba, Tuscany, Italy. *European Journal of Mineralogy,* **4**, 1085-1096

Ruggieri, G. and Gianelli, G. (1999) Multi-stage fluid circulation in a hydraulic fracture breccia of the Larderello geothermal field (Italy). *Journal of Volcanology and Geothermal Research,* **90**, 241-261

Ruggieri, G., Cathelineau, M., Boiron, M.C. and Marignac, C. (1999) Boiling and fluid mixing in the chlorite zone of the Larderello geothermal system. *Chemical Geology,* **154**, 237-256

Serri, G., Innocenti, F. and Manetti, P. (1993) Geochemical and petrological evidence of the subduction of delaminated Adriatic continental lithosphere in the genesis of the Neogene-Quaternary magmatism of central Italy. *Tectonophysics,* **223**, 117-147

Steele-MacInnis, M., Lecumberri-Sanchez, P. and Bodnar, R.J. (2012) HOCKIEFLINCS-H2O-NACL: A Microsoft Excel spreadsheet for interpreting microthermometric data from fluid inclusions based on the PVTX properties of H_2O-NaCl. *Computer Geoscience*, **49**, 334-337

Stefanini, B. and Williams-Jones, A.E. (1996) Hydrothermal evolution in the Calabona porphyry copper system (Sardinia, Italy): The path to an uneconomic deposit. *Economic Geology,* **91**, 774-791

Sterner, S.M., Hall, D.L. and Bodnar, R.J. (1988) Synthetic fluid inclusions. V. Solubility relations in the system NaCl-KCl-H_2O under vapor-saturated conditions. *Geochimica et Cosmochimica Acta,* **52**, 989-1006

Tanelli, G. (1983) Mineralizzazioni metallifere e minerogenesi della Toscana. *Memorie della Società Geologica Italiana*, **25**, 91-109

Tanelli, G., Morelli, F. and Benvenuti, M. (1993) I minerali del Campigliese: "beni ambientali, culturali e industriali." *Bollettino della Società Geologica Italiana,* **112**, 715-728

Valori, A., Cathelineau, M. and Marignac, C. (1992) Early fluid migration in a deep part of the Larderello geothermal field: a fluid inclusion study of the granite sill from well Monteverdi 7. *Journal of Volcanology and Geothermal Research,* **51**, 115-131

Vezzoni, S., Dini, A. and Rocchi, S. (2016) Reverse telescoping in a distal skarn system (Campiglia Marittima, Italy). *Ore Geology Review,* **77**, 176-193.

Wilson, J.W.J., Kesler, S.E., Cloke, P.L. and Kelly, W.C. (1980). Fluid inclusion geochemistry of the Granisle and Bell porphyry copper deposits, British Columbia. *Economic Geology*, **75**, 45-61

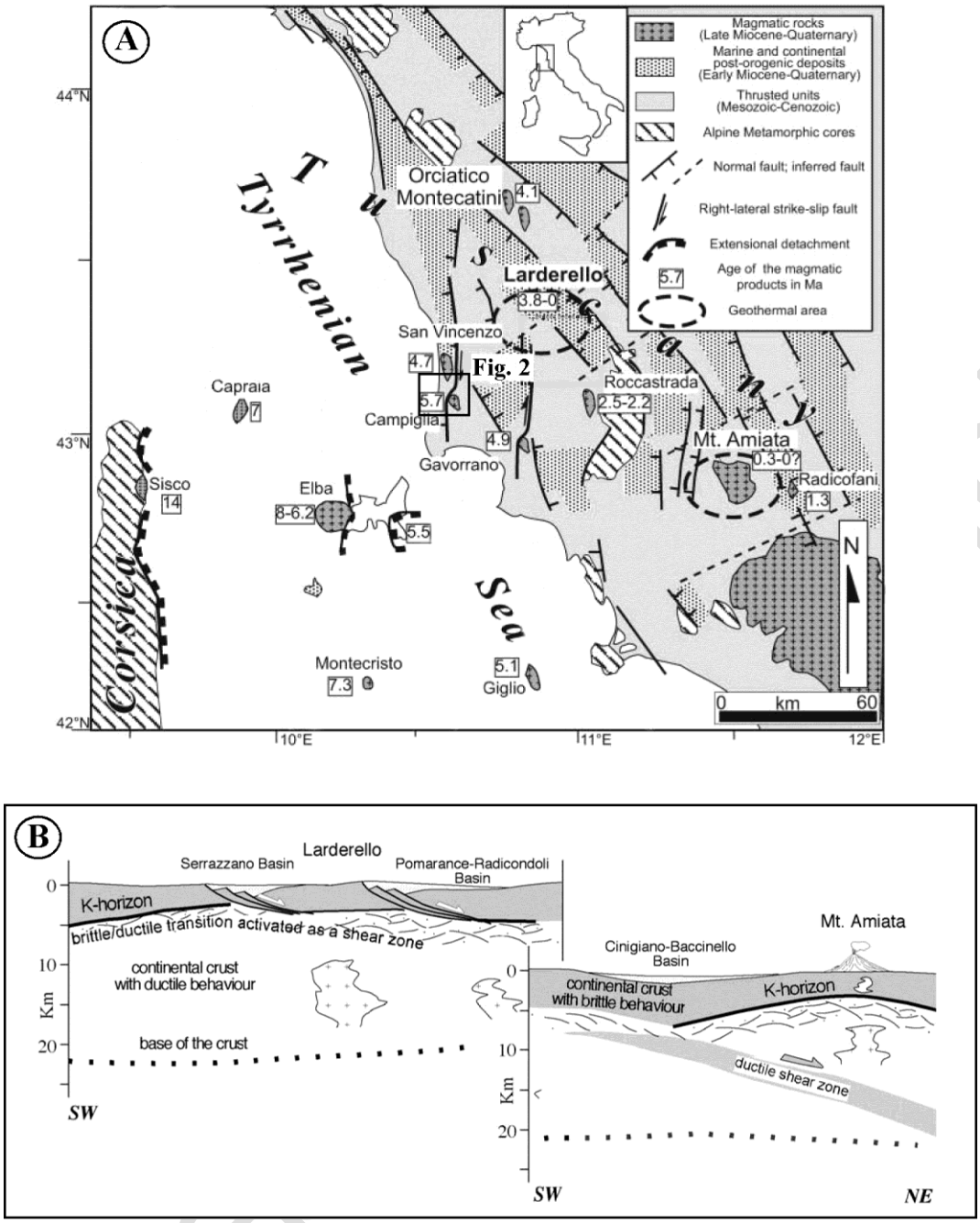

Fig. 1 Simplified tectonic map (A) of the northern Tyrrhenian area (after Rossetti *et al.*, 2008, modified), and geological sketch (B) of crustal structure in Southern Tuscany (after Brogi *et al.*, 2005 modified). The study area is within the box.

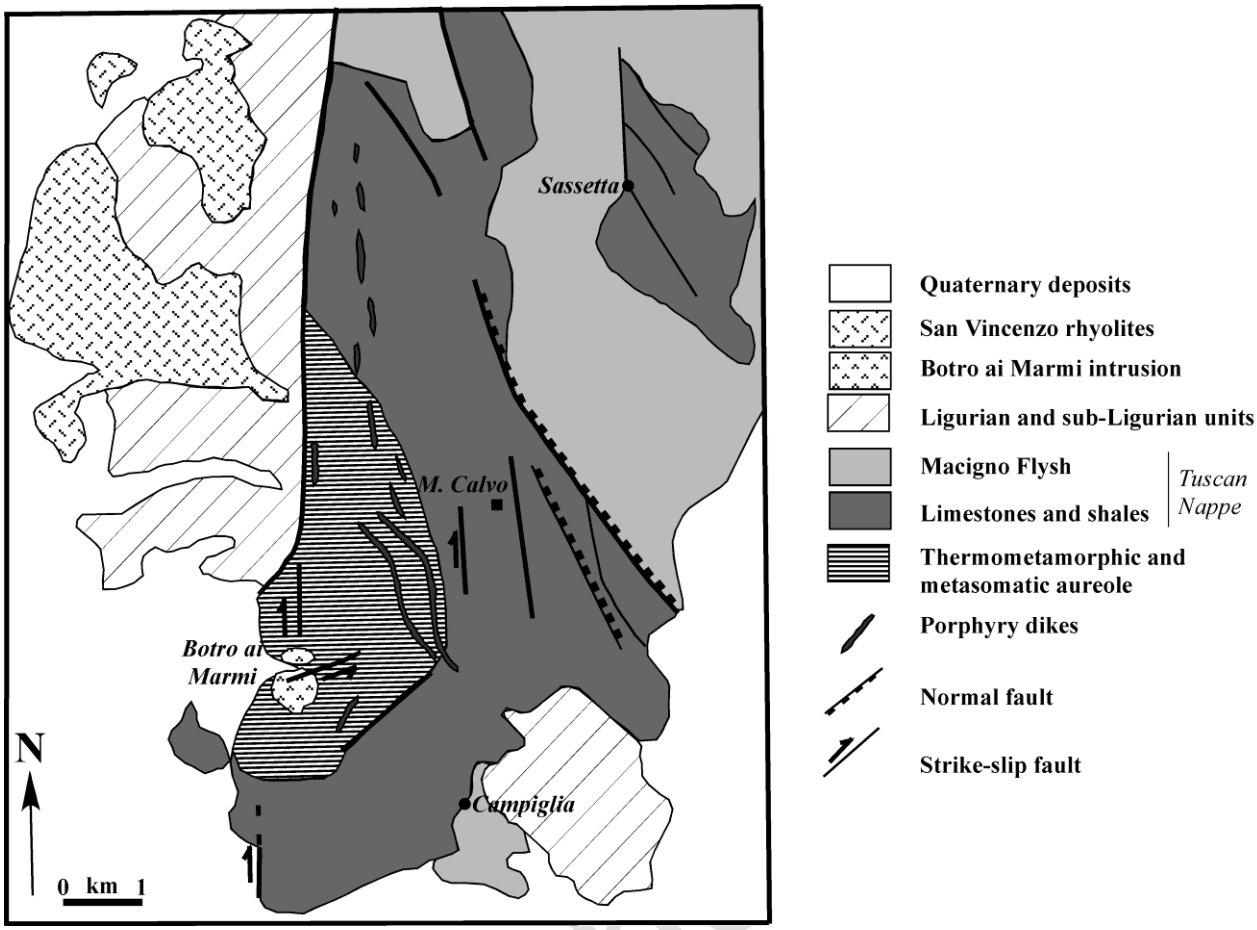

Fig. 2 Geological map of the Campiglia Ridge (modified after Rossetti *et al*., 2000).

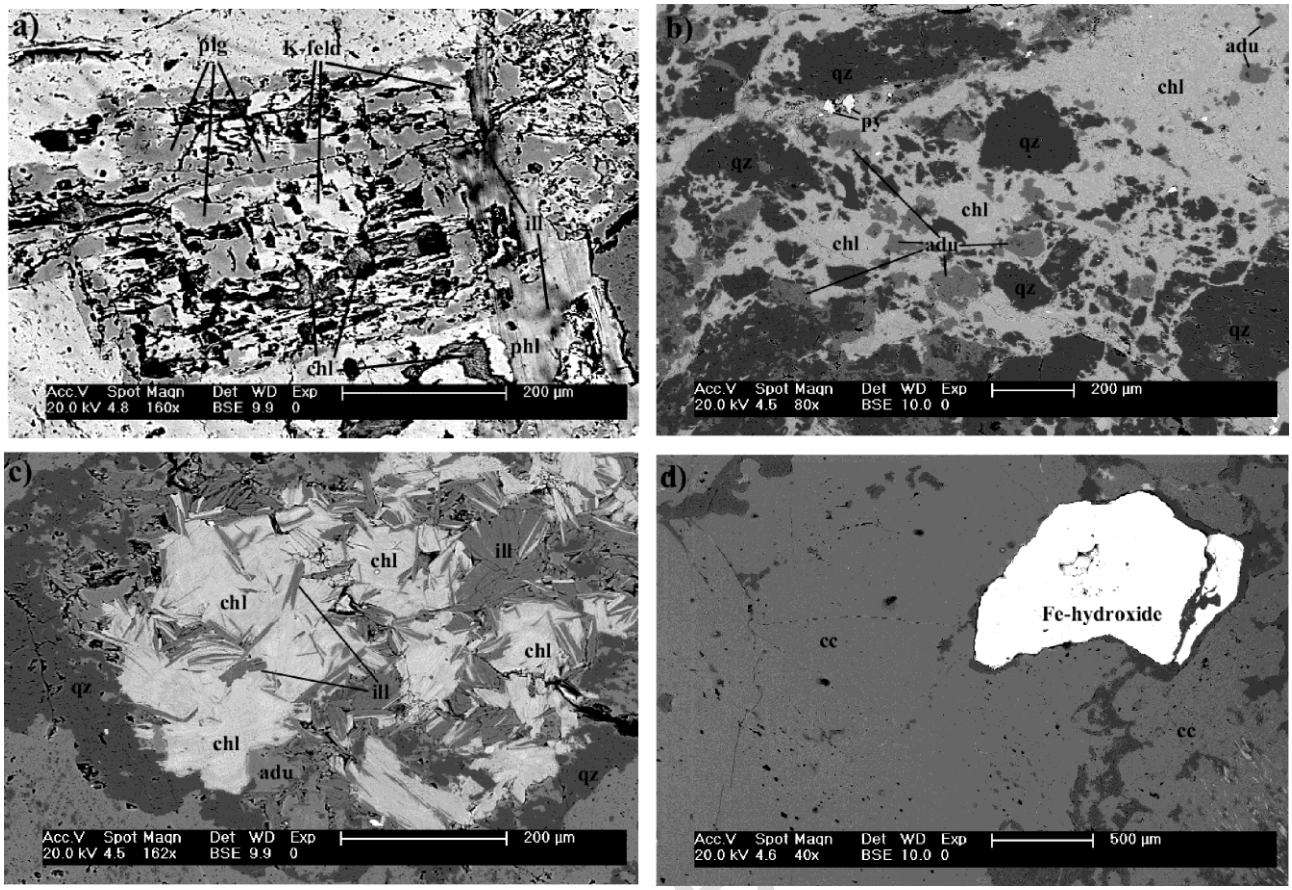

Fig. 3 Scanning electron microphotographs. a) Primary plagioclase altered by K-feldspar and phlogopite (potassic alteration facies). Chlorite and illite (propylitic alteration facies) partially overprint K-feldspar and phlogopite. b) Quartz + adularia + chlorite + pyrite vein (propylitic alteration) crosscuts the intrusive body. c) Pervasive propylitic alteration, made up of quartz + adularia + chlorite + illite, obliterates the primary mineralogical assemblage of quartz-monzonite intrusion. Abbreviations: plg = plagioclase, K-feld = K-feldspar, phl = phlogopite, chl = chlorite, ill = illite, qz = quartz, adu = adularia, py = pyrite, cc = calcite.

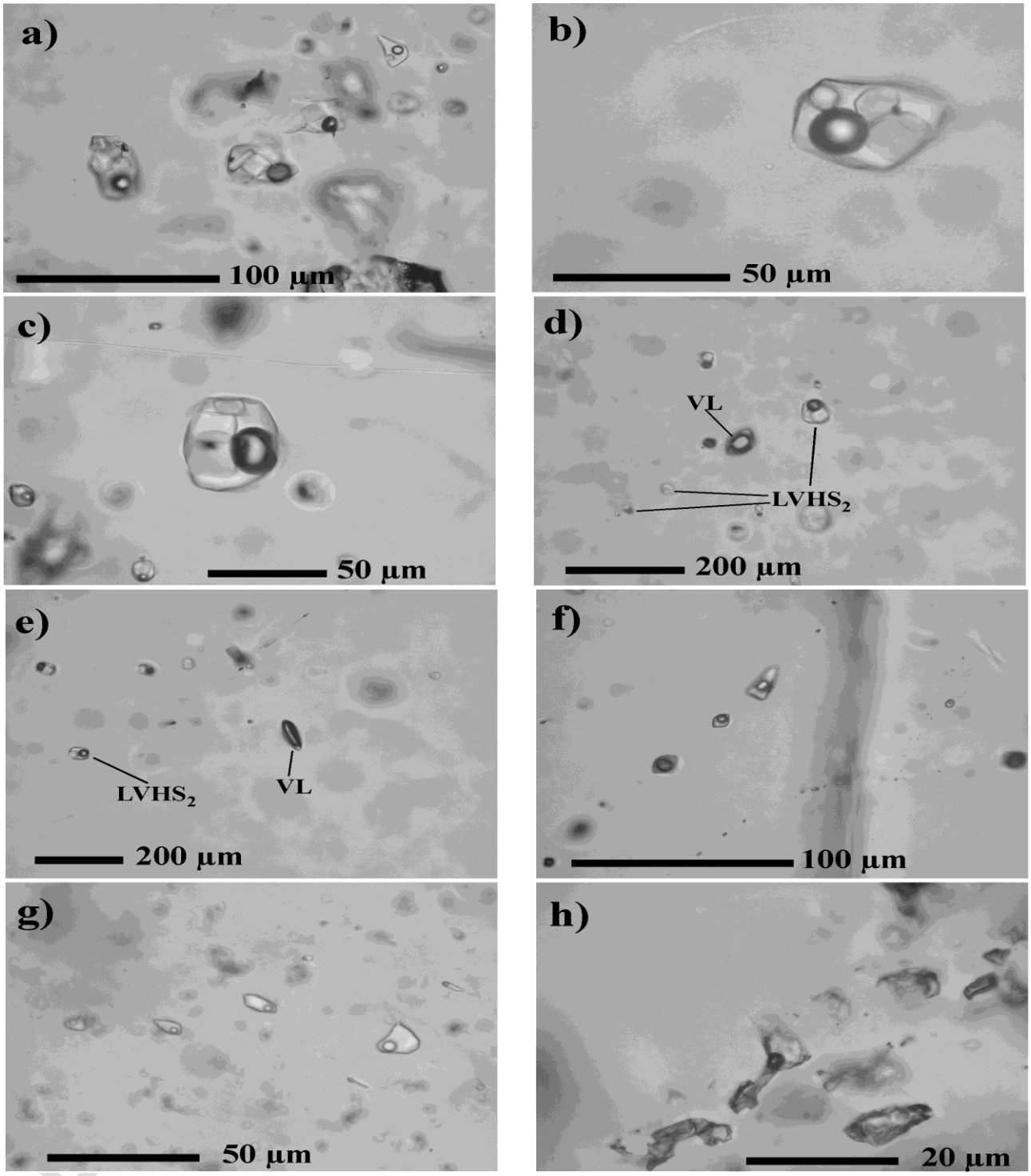

Fig. 4 Microphotographs of the different fluid inclusion types: (a, b, c) multiphase $LVHS_1$ primary fluid inclusions in quartz; (d, e) secondary trails of $LVHS_2$ multiphase and associated VL two-phase vapor-rich fluid inclusions in quartz; (f) secondary trail of LV_1 two-phase liquid-rich fluid inclusions in quartz; (g) secondary trail of LV_2 two-phase liquid-rich fluid inclusions in quartz; (h) LV_3 two-phase liquid-rich fluid inclusions in calcite.

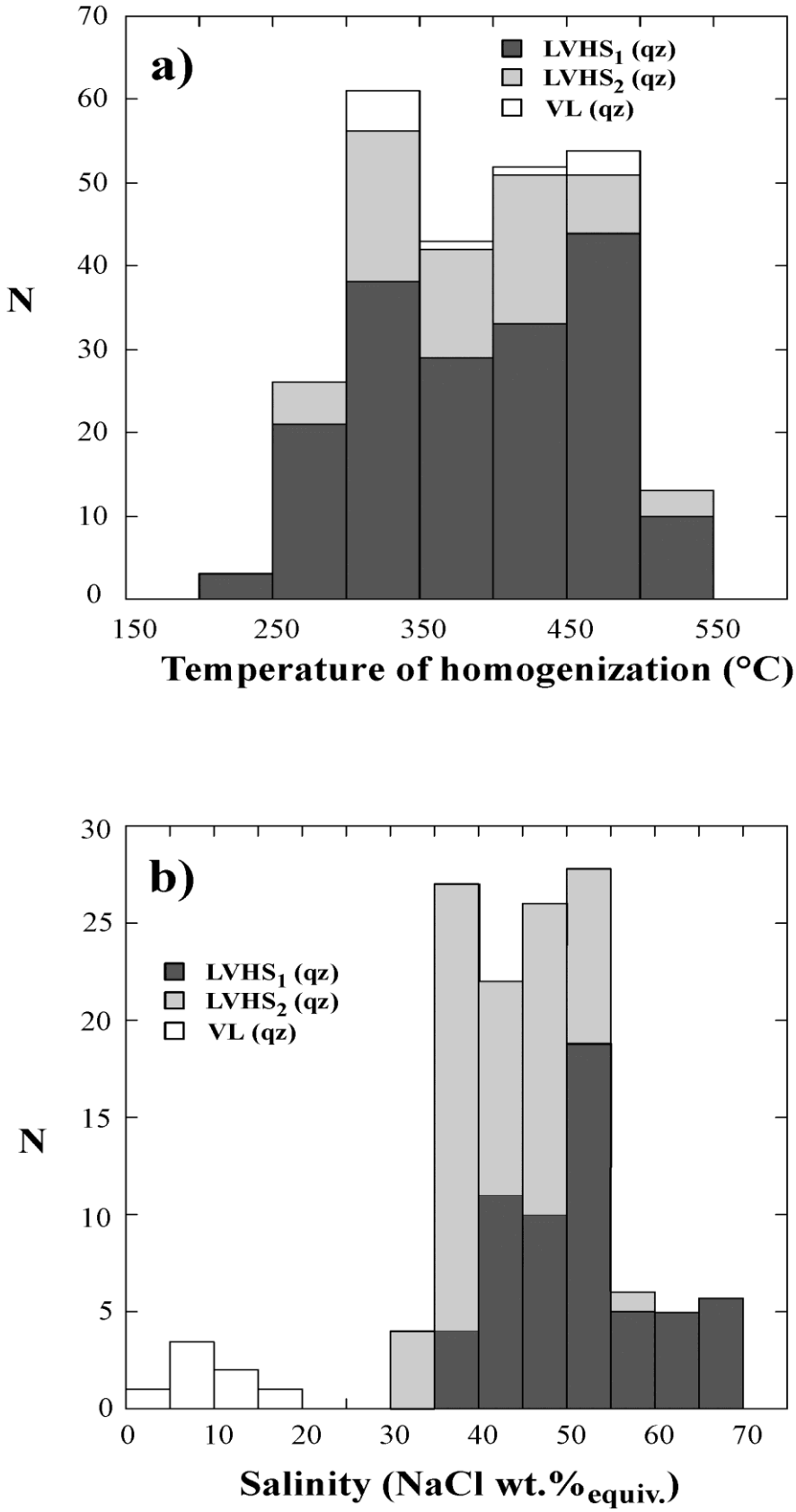

Fig. 5 Histograms of the homogenization temperatures (a) and salinities (b) of $LVHS_1$, $LVHS_2$ and VL fluid inclusions. N = number of measurements.

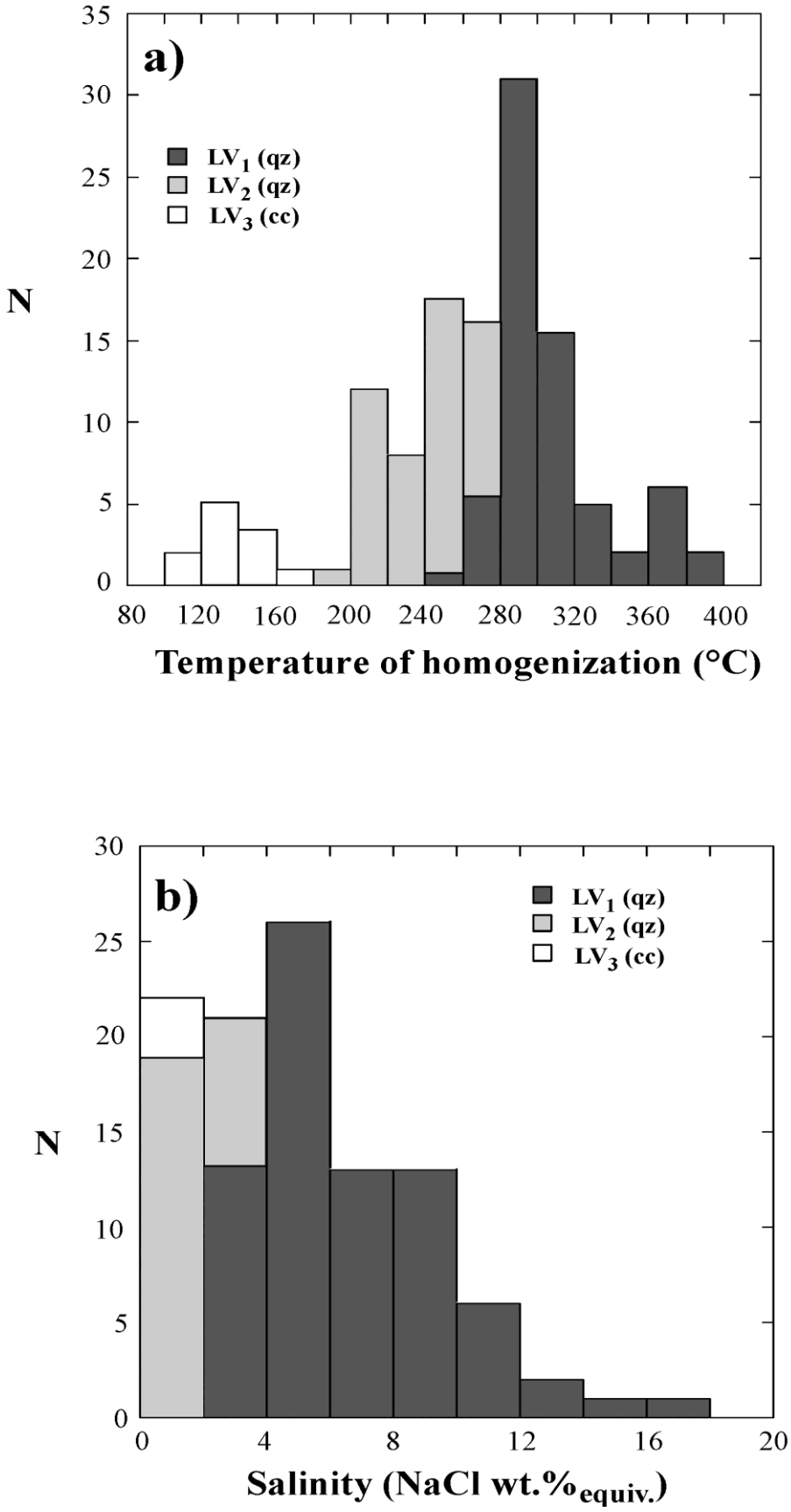

Fig. 6 Histograms of the homogenization temperatures (a) and salinities (b) of LV_1, LV_2 and LV_3 fluid inclusions. N = number of measurements.

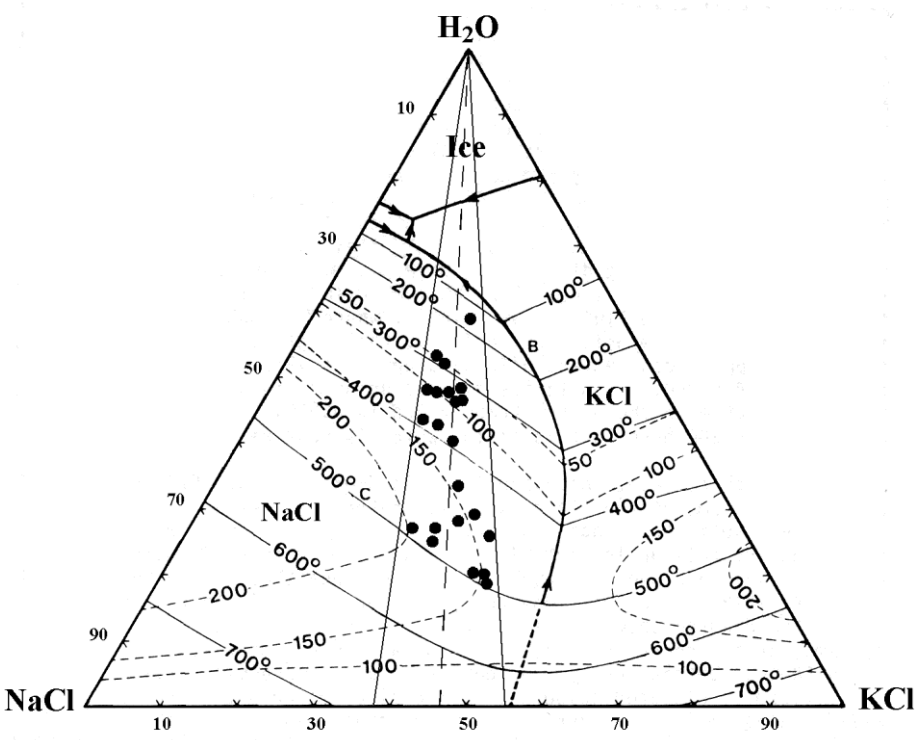

Fig. 7 NaCl-KCl-H_2O phase diagram showing the compositions of $LVHS_1$ fluid inclusions determined from the dissolution temperature of halite and sylvite. Phase diagram drawn after Roedder (1984).

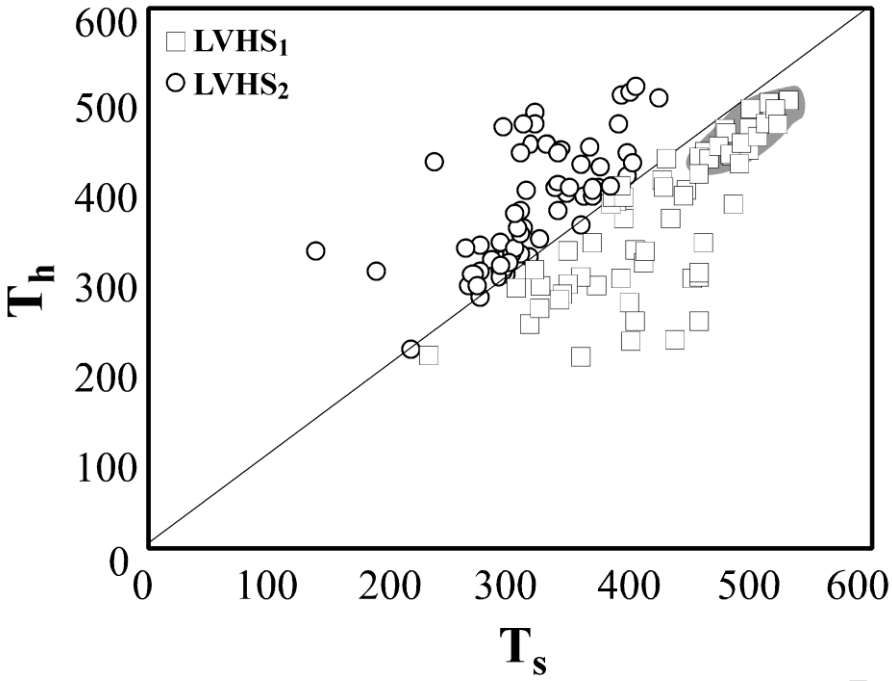

Fig. 8 Liquid-vapor homogenization temperature (T_h) vs. halite dissolution temperature (T_s) for LVHS fluid inclusions. The grey area is traced to identify the densest cluster, which is assumed to represent best the fluid trapped in $LVHS_1$ fluid inclusions.

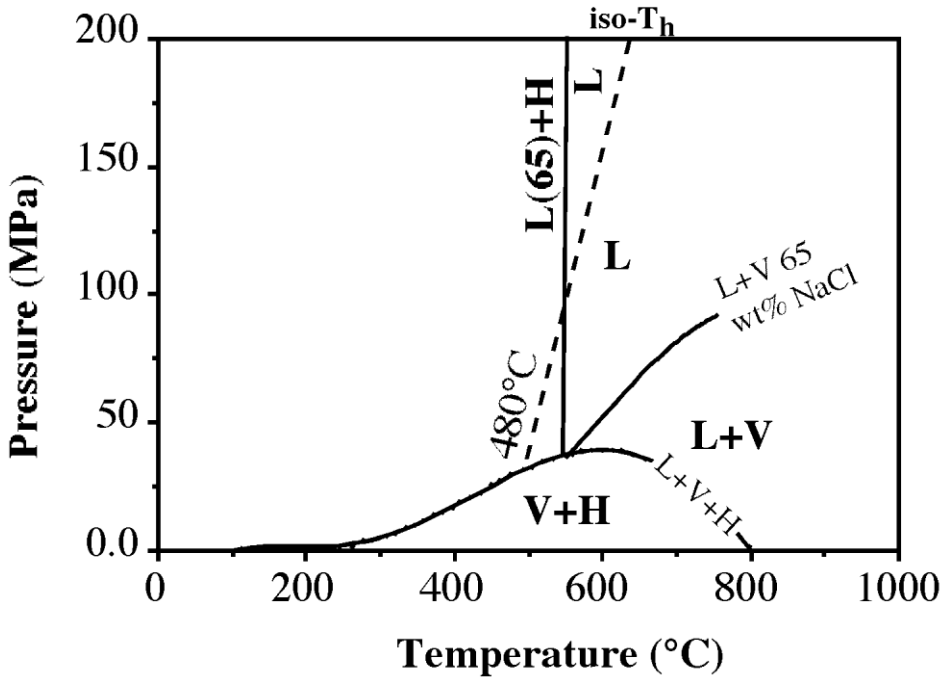

Fig. 9 Temperature-pressure diagram of part of the NaCl-H_2O system, illustrating trapping conditions for the dense cluster of data points (see Fig. 8) representing $LVHS_1$ fluid inclusions that exhibit average liquid-vapor homogenization at 500°C and that undergo final homogenization by halite dissolution at about 540°C corresponding to a salinity of 65 wt% $NaCl_{equiv.}$. The diagram shows the liquid + vapor + NaCl curve (L+V+H), the liquid + vapor curve (L+V) and corresponding liquidus (L+H) for 65 wt% $NaCl_{equiv.}$. The dashed line represents a constant liquid-vapor homogenization temperature (iso-$T_{h,}$ see Bodnar, 1994) for $LVHS_1$ fluid inclusions, which extends from the L+V+H curve at 500°C (representing the average T_h value of the densest cluster of data points in FIGURE 8). The intersection of the iso-T_h and the [L(65)+H] liquidus defines the minimum trapping pressure and temperature for the fluid in $LVHS_1$ fluid inclusions (around 90 MPa and 540°C).

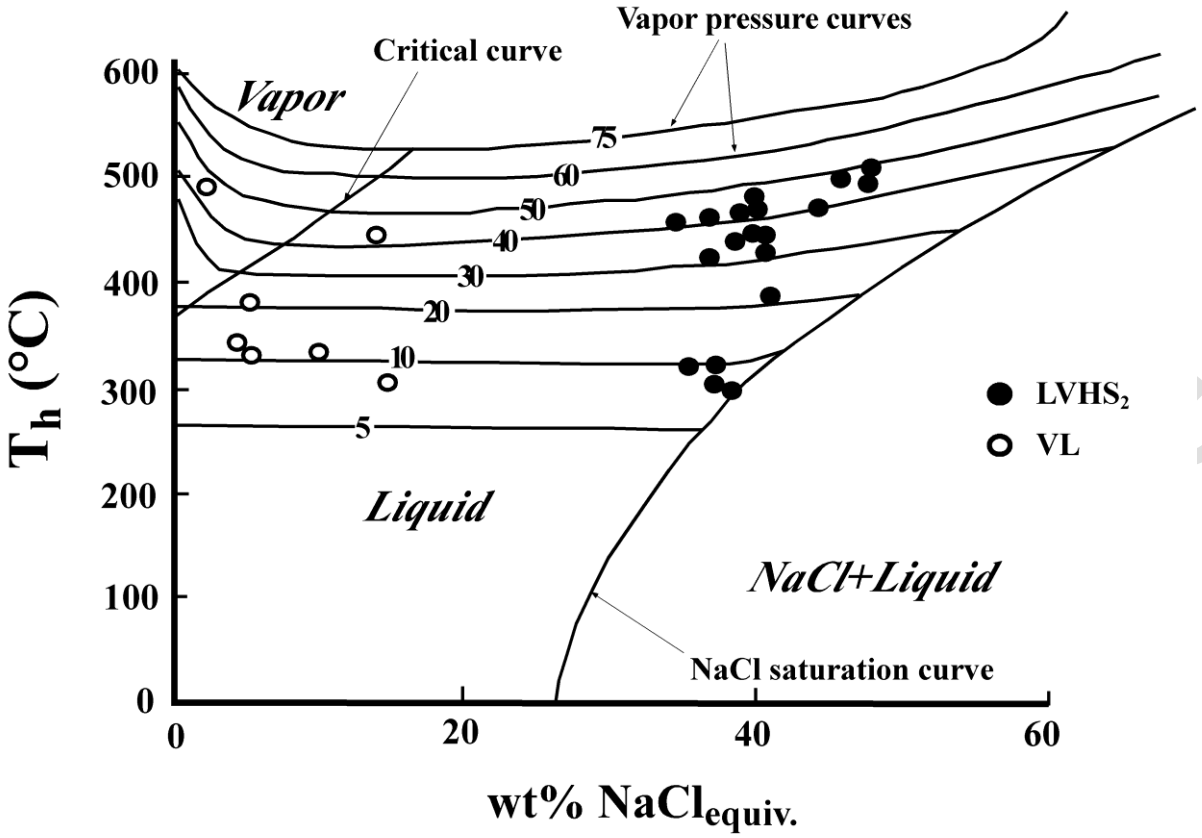

Fig. 10 Liquid-vapor homogenization temperature vs salinity of $LVHS_2$ and VL fluid inclusions plotted on a polybaric temperature-salinity projection of the system NaCl-H_2O. The halite saturation curve, critical curve and vapor pressure curves are after Chou (1987).

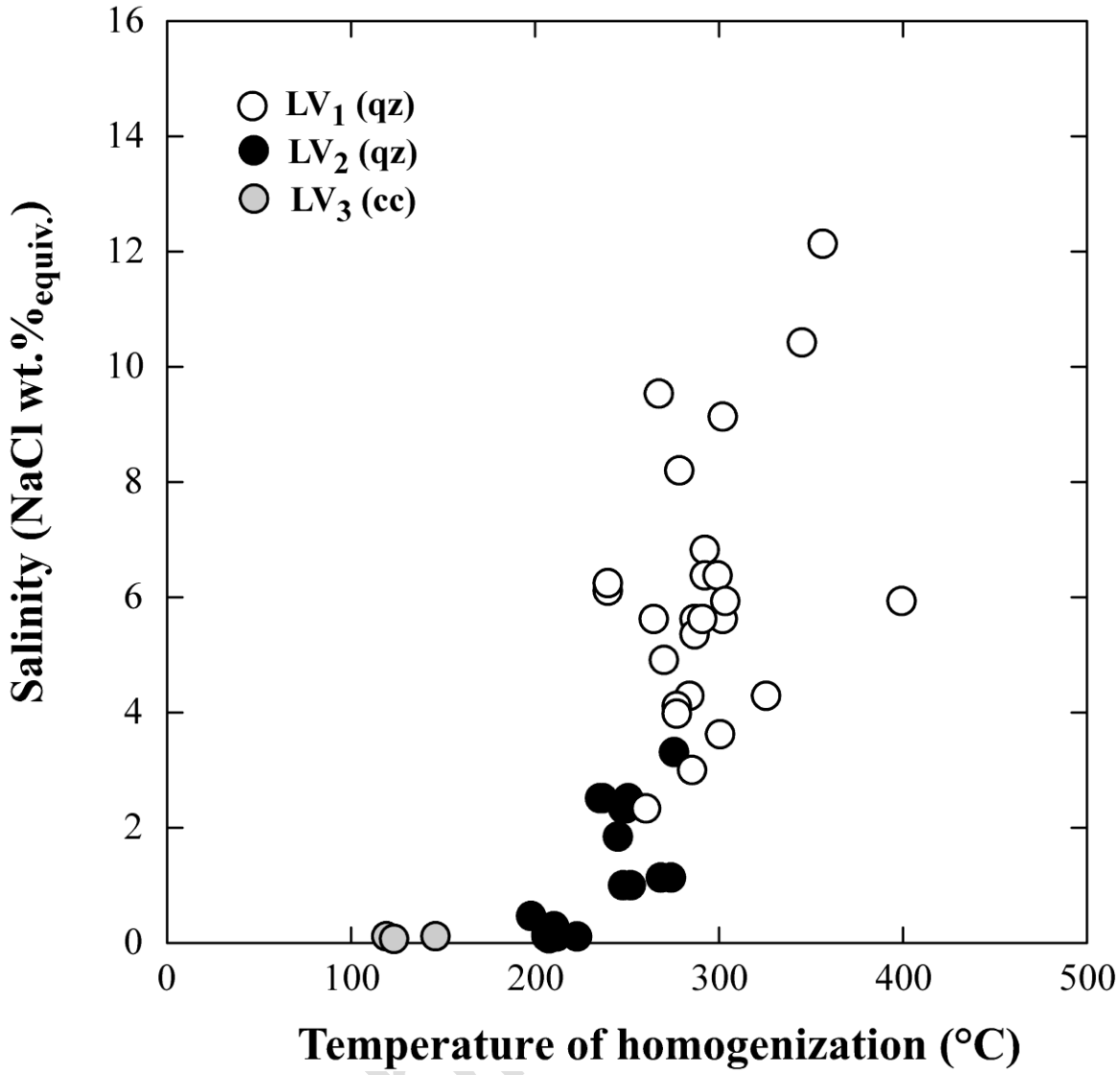

Fig. 11 Plot of homogenization temperature vs salinity of LV_1, LV_2 and LV_3 fluid inclusions.

Table 1 Representative analyses of phlogopite [1], illite [2], chlorite [3] and adularia [4].

	[1]	[1]	[2]	[2]	[3]	[3]	[3]	[3]	[4]	[4]
SiO_2	46.75	47.13	50.80	51.79	30.74	29.96	30.22	30.44	65.15	65.20
TiO_2	1.08	0.61	0.09	<ld	<ld	0.12	0.05	<ld	<ld	<ld
Al_2O_3	13.09	12.57	37.26	34.75	24.28	22.49	22.90	22.35	18.38	18.44
FeO	3.27	4.03	0.41	0.76	25.29	32.33	29.17	31.83	<ld	<ld
MnO	<ld	<ld	<ld	<ld	0.80	0.95	1.01	0.79	<ld	<ld
MgO	24.53	24.29	0.79	2.22	18.62	13.94	16.48	14.36	<ld	<ld
CaO	<ld	<ld	<ld	<ld	0.09	0.04	0.08	0.11	<ld	<ld
Na_2O	0.27	0.28	0.28	0.31	0.10	0.14	0.10	0.13	<ld	0.12
K_2O	11.00	11.08	10.37	10.17	0.07	0.04	<ld	<ld	16.47	16.25
sum	99.99	99.99	100.00	100.00	99.99	100.01	100.01	100.01	100.00	100.01
Si	6.24	6.31	6.34	6.48	5.58	5.64	5.60	5.71		
Al (IV)	1.76	1.69	1.66	1.52	2.42	2.36	2.40	2.29		
Al (VI)	0.11	0.29	3.82	3.60	2.77	2.63	2.60	2.65		
Ti	0.11	0.06	0.00	0.00	0.00	0.02	0.01	0.00		
Mn	0.00	0.00	0.00	0.00	0.12	0.15	0.16	0.12		
Fe^{2+}	0.36	0.45	0.04	0.08	3.84	5.09	4.52	4.99		
Mg	4.88	4.85	0.14	0.21	5.04	3.91	4.55	4.01		
Ca	0.00	0.00	0.00	0.00	0.02	0.01	0.02	0.02	0.00	0.00
Na	0.07	0.07	0.03	0.04	0.04	0.05	0.04	0.05	0.00	0.01
K	1.87	1.89	0.83	0.81	0.02	0.01	0.00	0.00	0.97	0.96
An									0	0
Ab									0	1
Or									100	99

Structural formulas have been calculated on the basis of: 22 oxygens for phlogopite and illite, 28 oxygens for chlorite and 8 oxygens for adularia; total iron has been considered as ferrous.
<ld = below detection limit.
Analyses have been carried out by SEM-EDS using a Philips XL30 apparatus coupled with EDAX Genesis micro-analytical system (Earth Science Department, University of Pisa) at 20kV accelerating energy and 0.1 nA beam current. Before each analytical session, calibration and standardization using international mineral standards were performed. Analyses are normalised to 100 due to EDAX software used.

Table 2 Summary of fluid inclusion data.

Inclusion type		T_e	T_{mi}	T_{cd}	$T_{S\text{-}KCl}$	$T_{S\text{-}NaCl}$	*Salinity*[1]	T_{hom}
Multiphase liquid-rich fluid inclusions (LVHS)	$LVHS_1$	-35/-40°C [45]			100÷455°C [26]	300÷575°C [59]	38÷70 [59]	245÷522°C [177]
	$LVHS_2$	-35/-40°C [25]			140÷250°C [5]	240÷470°C [74]	34÷56 [74]	280÷510°C [52]
Two phase liquid-rich fluid inclusions (LV)	LV_1	-35/-40°C [56]	-1.3/-12.2°C [75]				2.2÷16.1 [75]	250÷400°C [70]
	LV_2	-21/-23°C [18]	-0.1/-1.5°C [27]				0.2÷2.5 [27]	195÷265°C [47]
	LV_3	-35/-40°C [3]	-0.0/-0.1°C [3]				0.1÷0.2 [3]	100÷165°C [12]
Two phase vapor-rich fluid inclusions (VL)		nd		2.1÷10.0 [7]			2÷17 [7]	328÷488°C [10]

T_e = temperature of first ice melting **$T_{s\text{-}NaCl}$** = temperature of halite homogenization **$T_{s\text{-}KCl}$** = temperature of sylvite homogenization **[]** = number of measurements
T_{mi} = temperature of final ice melting **T_{hom}** = temperature of vapor bubble homogenization **T_{cd}** = temperature of clathrate dissociation **nd** = not determined
1 Salinity is reported as wt% $NaCl_{equiv.}$